Journal of Power Sources 241 (2013) 355–358

Contents lists available at SciVerse ScienceDirect

Journal of Power Sources

journal homepage: www.elsevier.com/locate/jpowsour

Short communication

In situ neutron-diffraction study of the $Ti_{38}V_{30}Cr_{14}Mn_{18}$ structure during hydrogenation

Yang Fei [a,*], Xiangcheng Kong [b], Zhu Wu [c], Huanhuan Li [a], V.K. Peterson [d]

[a] *Automotive Engineering Research Institue, Jiangsu University, 301 Xuefu Road, Zhenjiang 212013, PR China*
[b] *Energy Efficiency Office of Zoucheng Municipal People's Government, 1556 West Taiping Road, Zoucheng, Shandong 273500, PR China*
[c] *Shanghai Institute of Microsystem and Information Technology, Chinese Academy of Sciences, Shanghai 200050, PR China*
[d] *Australian Nuclear Science and Technology Organization, Lucas Heights, NSW, Australia*

HIGHLIGHTS

- We studied phase transformations of $Ti_{38}V_{30}Cr_{14}Mn_{18}$ by *in situ* neutron powder diffraction.
- The structure change from BCC to FCC though BCT phase during sorption process.
- GSAS Rietveld confirmed the D_2 atoms occupied the octahedral position of BCC phase.
- The D_2 atoms occupied the tetrahedral position of BCT, FCC phase.

ARTICLE INFO

Article history:
Received 21 December 2012
Received in revised form
18 March 2013
Accepted 23 April 2013
Available online 9 May 2013

Keywords:
Hydrogen storage alloy
Ti–V–Cr–Mn alloy
In situ neutron-diffraction
Phase transformation

ABSTRACT

The phase transformations of the $Ti_{38}V_{30}Cr_{14}Mn_{18}$ alloy during hydrogenation and dehydrogenation using deuterium (D_2) were investigated using *in situ* neutron powder diffraction (NPD) at various D_2 pressures up to 2 MPa. Initially, the first hydride that formed, $Ti_{38}V_{30}Cr_{14}Mn_{18}D_{15}$, had the same body centered cubic (BCC) crystal structure as the starting alloy. Upon further hydrogenation, the system displays a distinct two-phase mixture of the intermediate BCC and body-centered tetragonal (BCT) phases, that exist in a ration of 1.38:1.42, respectively. At the end of the deuterium absorption, the phase pure $Ti_{38}V_{30}Cr_{14}Mn_{18}D_{183}$ material forms, with a face-centered cubic (FCC) structure. Upon dehydrogenation, all hydride phases eventually returned to the initial alloy phase without any amorphization or disproportionation. Using standard Rietveld refinement, information on the variation of the deuterium site occupancy, the lattice symmetry, and the cell volume were determined during these phase changes and are presented.

1. Introduction

BCC TiV-based alloys have been shown to exhibit excellent effective hydrogen storage capacities and a plateau pressure in the pressure–composition (P–C) hydrogen absorption and desorption isotherm [1–4]. To date, research into these alloys is mainly focused on improving their hydrogen storage capacities and electrode characteristics [5–12]. Hydrogen absorption and desorption properties of metal hydrides are closely related to their crystal structure, involving the occupation of hydrogen at interstitial sites in the structure. However, experimental studies concerning the location of hydrogen atoms in these materials are relatively rare as a result of the difficulty of many measurement techniques in accurately locating hydrogen in the crystal structure. The deep penetration capability of neutrons into most metallic materials makes neutron diffraction a unique and powerful technique for the investigation of alloy structure [13]. Importantly, hydrogen site occupation can be directly determined only by neutron diffraction [14], with *in situ* neutron powder diffraction an effective way to investigate hydrogen (i.e., deuterium) occupation in various hydriding states of a material.

Recently, Denys et al. found that the saturated $La_2MgNi_9D_{13}$ hydride contained a structure in which H atoms favor occupation of Mg-surrounded sites within the $LaMgNi_4$ slabs, triangles [$MgNi_2$], and tetrahedra [$LaMgNi_2$], using *in situ* neutron diffraction, with a local hydrogen ordering taking place with respect to the hydrogen sub-lattice that is built from a stacking of the MgH_6 octahedra and NiH_4 tetrahedra [15].

* Corresponding author.
E-mail address: yang_fei@yahoo.com (Y. Fei).

0378-7753/$ – see front matter © 2013 Elsevier B.V. All rights reserved.
http://dx.doi.org/10.1016/j.jpowsour.2013.04.118

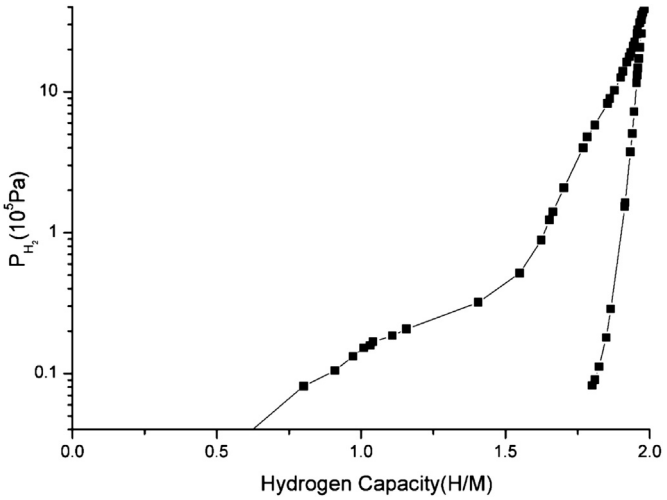

Fig. 1. Pressure-composition isotherm of $Ti_{38}V_{30}Cr_{14}Mn_{18}$ at 298 K.

In this paper we detail the occupation of hydrogen in the $Ti_{38}V_{30}Cr_{14}Mn_{18}D_x$ material during both hydrogen absorption and desorption using *in situ* neutron powder diffraction, and evaluate the material's lattice parameter, lattice strain, and mass fraction of the constituent phases during these processes using Rietveld analysis.

2. Experimental procedures

$Ti_{38}V_{30}Cr_{14}Mn_{18}$ was prepared using magnetic levitation melting in an argon atmosphere, with the ingot being turned and remelted four times to ensure homogeneity and to avoid oxidation. After remelting, the mixture was annealed for 5 h in an argon atmosphere at 773 K and then crushed into powder that sieved through a 100 mesh sieve. *In situ* neutron powder diffraction (NPD) of the $Ti_{38}V_{30}Cr_{14}Mn_{18}$ material was performed using the High-Intensity Powder Diffractometer (WOMBAT) [16] at the Open Pool Australian Light-water (OPAL) reactor facility at the Australian Nuclear Science and Technology Organisation (ANSTO). A Ge(113) monochromators reflection with a 90° take-off angle was selected to produce a wavelength of 2.419 Å and provide a compromise between resolution, d-spacing range, and neutron flux. Data were collected for 10 min in the scattering angle range $15 \leq 2\theta \leq 135°$. WOMBAT features an area detector covering 120° in scattering angle (2θ), effectively enabling diffraction data to be continuously collected during hydrogen charging/discharging. The sample was placed in a 316 stainless steel container with a wall thickness of 0.2 mm and an inner diameter of 6 mm, and sealed using a VCR type fitting with a stainless steel lid fitted with a stainless steel capillary with a bellows-sealed VCR valve. This was connected (using another VCR fitting) to a gas delivery system composed of a stainless steel dosing volume fitted with a high-accuracy pressure transducer, which was connected via two separate bellows-sealed VCR valves to a 60 bar 99.999% purity D_2 cylinder and a turbo-vacuum device, with heating achieved using an in-house produced furnace featuring infra-red heating lamps as per previous experiments [17]. The initial alloy sample was activated in vacuum at 573 K for 10 min and charged with deuterium gas at 293 K until pressure equilibration was reached. Upon dehydriding, NPD data were collected after the pressure was slowly lowered until stability was achieved. As a consequence of the lower desorption plateau for the material, the materials was heated whilst under vacuum in order to achieve complete hydrogen desorption. A stable vacuum of approximately 7×10^{-5} Pa was achieved during sample evacuation. Data correction and reduction were undertaken using the program LAMP [18]. Rietveld refinements were carried out using the GSAS [19] suite of programs with the EXPGUI [20] interface.

3. Results and discussion

In the previous hydrogen sorption isotherms studies of the $Ti_{38}V_{30}Cr_{14}Mn_{18}$–$H_2$ system, the results shown two plateaus at pressures of approximately 0.01×10^5 Pa and 0.2×10^5 Pa at 298 K [21]. A maximum hydrogen storage capacity of approximately 2 H/M was achieved on prepared sample material as presented in Fig. 1.

Fig. 2 shows the evolution of the NPD profiles during hydrogen absorption in the $Ti_{38}V_{30}Cr_{14}Mn_{18}$ alloy from the empty- to fully-hydrided state. The stainless steel container contributes significantly to the data, with two large reflections clearly visible at 72 and 85° 2θ. A solid solution of hydrogen in the intermetallic alloy, $Ti_{38}V_{30}Cr_{14}Mn_{18}D_x$, starts to form immediately after hydrogen is introduced into the sample cell. This leads to a slight shift of reflections associated with the alloy toward lower 2θ angles, indicating a lattice expansion. The intensity of the 200 and 220 reflections also increases significantly with the introduction of D_2 (Fig. 2a). During this process, a new hydride 110 reflection appears at around 67° 2θ, the intensity of which increases initially and then decreases, before disappearing, as D_2 gas is added (Fig. 2b). The NPD data show that the initial phase, BCC $Ti_{38}V_{30}Cr_{14}Mn_{18}$, gradually transforms into an FCC phase as the deuterium content in the sample increases. It is known that Ti–V–Mn alloys with a BCC crystal structure will transform to an FCC structure upon hydrogenation [22,23], and hence, the NPD data are consistent with deuteration of the sample. The evolution of the NPD profiles during dehydriding show a reverse process to the hydriding process

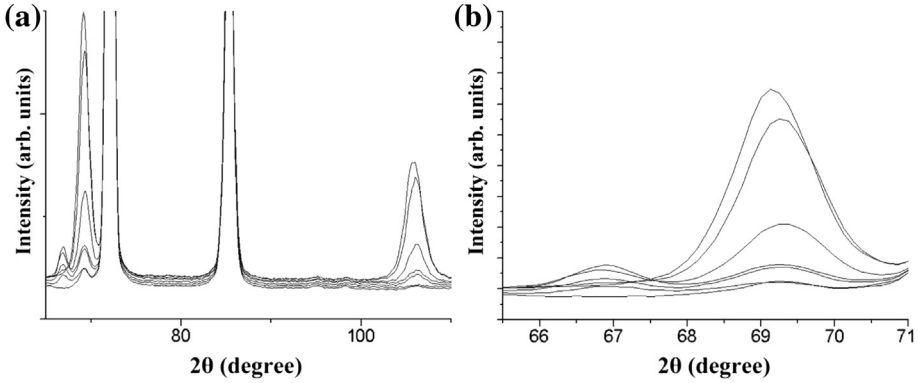

Fig. 2. (a) Select region of NPD data of $Ti_{38}V_{30}Cr_{14}Mn_{18}D_x$ during hydriding, with (b) detailing the 65–71° 2θ region.

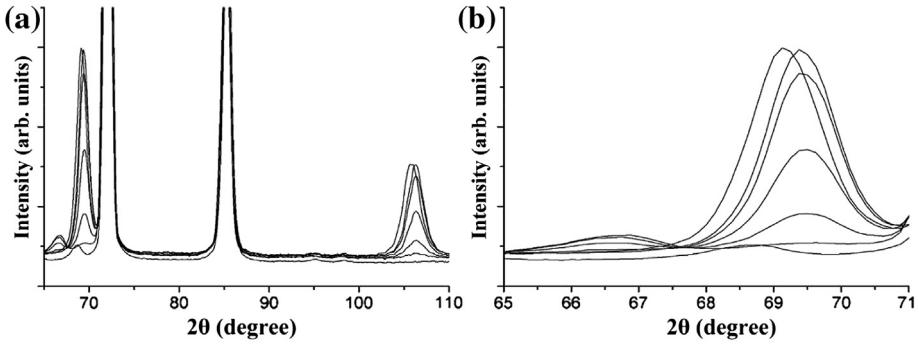

Fig. 3. (a) Select region of NPD data of $Ti_{38}V_{30}Cr_{14}Mn_{18}D_x$ during dehydriding, with (b) detailing the 65–71° 2θ region.

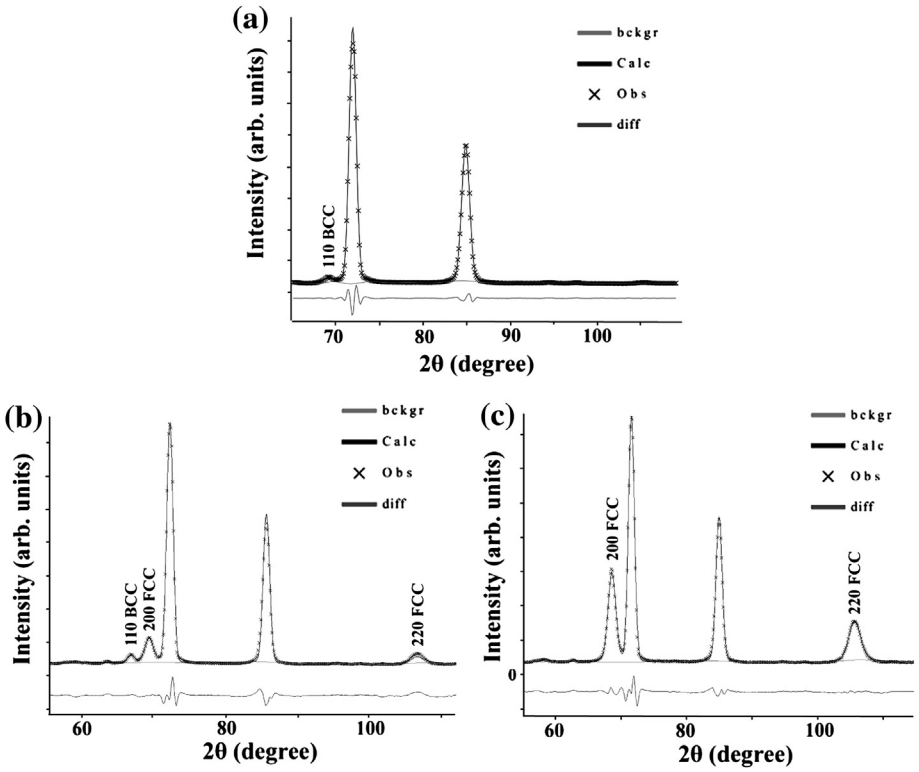

Fig. 4. Rietveld refinement plots using NPD data of the Ti–V–Mn hydride (a) $Ti_{38}V_{30}Cr_{14}Mn_{18}$, (b) $Ti_{38}V_{30}Cr_{14}Mn_{18}D_{24}$, and (c) $Ti_{38}V_{30}Cr_{14}Mn_{18}D_{183}$.

(Fig. 3), with the hydride peaks shifting toward higher 2θ and 200 and 220 reflection intensities decreasing with reduced deuterium content (Fig. 3a). Similarly, a new hydride 110 reflection appears, before disappearing as the deuterium content further decreases (Fig. 3b). These NPD data are therefore consistent with the process of dehydrogenation of Ti–V–Mn alloys, where the FCC crystal structure transforms to a BCC structure [24].

During Rietveld refinement, no soft constrain was used, and Gaussian profile function was used for the neutron diffraction analysis. The corresponding Rietveld refinement plots using NPD data of the hydriding material are shown in Fig. 4. Rietveld refinements further confirm that there are three phases that form during the hydriding process. The first phase (I) has a BCC structure and forms for deuterium contents less than 0.15 D/M. The NPD data for this

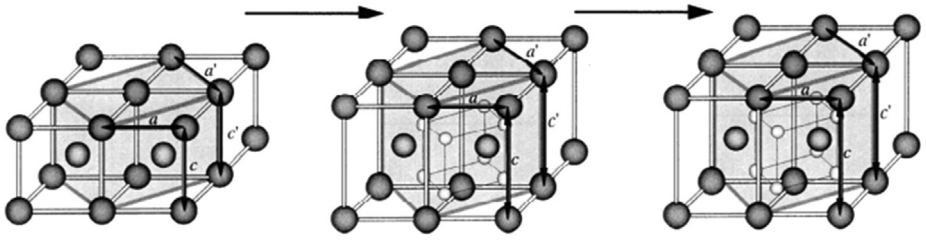

Fig. 5. Change of the crystal structure of the metal lattice from the BCC, to the BCT, and then to the FCC structure during hydrogenation.

phase feature broad reflections (Fig. 4a). The second hydride phase (II) has a deformed BCC structure, formally a BCT structure. Notably, in the V–H system, the metal sub lattice of the monohydride phase β-V_2H has a BCT structure with c/a ratio of approximately 1.1 [25]. This second phase is transitional in nature (Fig. 4b), with the fully-hydrided phase (III) adopting an FCC structure (Fig. 4c).

Further studies were undertaken to establish the influence of the deuterium content on the phase. When the deuterium content is less than 0.15 D/M, the $Ti_{38}V_{30}Cr_{14}Mn_{18}D_x$ alloy is phase pure BCC structure as per the pristine undeuterated material. The lattice constant for this material is 0.3044(6) nm with error as shown in the parenthesis. During deuteration, the alloy structure changes by expansion along the unit cell c direction. When the deuterium content reached 0.24 D/M, two phases formed in the structure, with deuterium atoms occupying in the interstitial octahedral sites of the BCC structure (I) and tetrahedral sites of the BCT structure (II). These two phases coexist in a ratio of 1.38: 1.42, respectively. In the hydride (I), a relatively small lattice expansion is observed relative to the pristine material, with the lattice constant and statistical errors in the parenthesis being 0.3138(3) nm. In the hydride (II) the lattice constants are $a = b = 0.3138(3)$ nm, and $c = 0.4293(5)$ nm. Hydrate (I) has deuterium atoms at the (*0, 0.5, 0.5*) octahedral site with an occupancy of ~0.05. In hydride (II), deuterium atoms at the (0.25, 0.25, 0.25) tetrahedral site have an occupancy of ~0.27. This result indicates that deuterium atoms first enter into the octahedral sites of the BCC alloy structure in hydrogen absorption process, where the material expands along the c axis of the unit cell as the deuterium content increases. Consequently, deuterium atoms finally occupy both octahedral sites within the BCC structure and tetrahedral sites of the BCT structure that forms as a second phase. A final hydrogen content of 1.83 D/M is reached, slightly higher than that obtained from the pressure–composition isotherm, most likely as a result of the lower pressure achieved in the NPD experiment. The fully-hydrogenated alloy in the NPD experiment can be ascribed the general formula $Ti_{38}V_{30}Cr_{14}Mn_{18}D_{183}$, which is a single phase FCC structure, hydrate (III). In hydrate (III) deuterium atoms are located at tetrahedral sites (0.25, 0.25, 0.25) with an occupancy of ~ 0.915 and a lattice constant 0.433 nm with final refined Rwp error $< 3.556\%$.

The NPD study reveals phase transitions in the hydrogen absorption process of the $Ti_{38}V_{30}Cr_{14}Mn_{18}$ alloy as shown in Fig. 5. As the hydrogen content increases, the structure of the alloy changes from BCC to an FCC phase via an intermediate BCT phase.

4. Conclusion

In conclusion, $Ti_{38}V_{30}Cr_{14}Mn_{18}$ has an excellent hydrogen storage capacity amongst the characterized representatives of the hybrid Ti–V–Mn compounds, which are used in nickel–metal hydride batteries. Neutron diffraction studies of the $Ti_{38}V_{30}Cr_{14}Mn_{18}$ alloy during hydrogenation reveal that the alloy structure completely transforms from the initial BCC structure to the FCC structure via an intermediate BCT phase, and that this process is completely reversible upon dehydrogenation. Rietveld structural analyses confirm that the deuterium atoms are located at octahedral sites of the BCC phase and at tetrahedral sites of the BCT and FCC phases.

Acknowledgment

This work is supported by the National “863 program” (No. 2007AA05Z149) and Science and Technology Commission of Shanghai Municipality (No. 09dz1206800).

References

[1] S.W. Cho, G.C. Shim, G.S. Choi, C.N. Park, J.H. Yoo, J. Choi, J. Alloys Compd. 430 (2007) 136–141.
[2] S.-W. Cho, C.-N. Park, J.-H. Yoo, J. Choi, J.-S. Park, C.-Y. Suh, G. Shim, J. Alloys Compd. 403 (2005) 262–266.
[3] X.B. Yu, J.Z. Chen, Z. Wu, B.J. Xia, N.X. Xu, Int. J. Hydrogen Energy 29 (2004) 1377–1381.
[4] T. Tamura, A. Kamegawa, H. Takamura, M. Okada, Mater. Trans. 44 (2003) 641–644.
[5] X.B. Yu, G.S. Walker, D.M. Grant, Z. Wu, B.J. Xia, J. Shen, Appl. Phys. Lett. 87 (2005) 133121-1–133121-3.
[6] H. Liang, Y. Chen, Y. Yan, C. Wu, M. Tao, Mater. Sci. Eng. A 459 (2007) 204–208.
[7] T. Dou, Z. Wu, J. Mao, N. Xu, Mater. Sci. Eng. A 476 (2007) 34–38.
[8] T. Tamura, Y. Tominaga, K. Matsumoto, T. Fuda, T. Kuriiwa, A. Kamegawa, H. Takamura, M. Okada, J. Alloys Compd. 330-332 (2002) 522–525.
[9] T. Kuriiwa, T. Maruyama, A. Kamegawa, M. Okada, Int. J. Hydrogen Energy 35 (2010) 9082–9087.
[10] M. Shibuya, J. Nakamura, E. Akiba, J. Alloys Compd. 466 (2008) 558–562.
[11] M. Shibuya, J. Nakamura, H. Enoki, E. Akiba, J. Alloys Compd. 475 (2009) 543–545.
[12] J. Matsuda, Y. Nakamura, E. Akiba, J. Alloys Compd. 509 (2011) 4352–4356.
[13] C.G. Winsor, Pulsed Neutron Scattering, Taylor and Francis, London, 1981.
[14] Y. Nakamura, R.C. Bowman Jr., E. Akiba, J. Alloys Compd. 431 (2007) 148–154.
[15] R.V. Denys, V.A. Yartys, C.J. Webb, Inorg. Chem. 51 (2012) 4231–4238.
[16] A.J. Studer, M.E. Hagen, T.J. Noakes, Phys. B 385–386 (2006) 1013–1015.
[17] M. Paskevicius, D.A. Sheppard, A.-L. Chaudhary, C.J. Webb, E. Mac, A. Gray, H.Y. Tian, V.K. Peterson, C.E. Buckley, Int. J. Hydrogen Energy 36 (2011) 10779–10786.
[18] D. Richard, M. Ferrand, G.J. Kearley, J. Neutron Res. 4 (1996) 33–39.
[19] A.C. Larson, R.B. Von Dreele, General Structure Analysis System (GSAS), Los Alamos National Laboratory Report LAUR 86–748 (1994).
[20] B.H. Toby, J. Appl. Crystallogr. 34 (2001) 210–213.
[21] Kei Nomura, Etsuo Akiba, J. Alloys Compd. 231 (1995) 513–517.
[22] E. Akiba, Y. Nakamura, Met. Mater. Int. 7 (2001) 165–168.
[23] Y. Nakamura, E. Akiba, J. Alloys Compd. 311 (2000) 317–321.
[24] S. Miraglia, D. Fruchart, N. Skryabina, M. Shelyapina, B. Ouladiaf, E.K. Hlil, P. de Rango, J. Charbonnier, J. Alloys Compd. 442 (2007) 49–54.
[25] H. Asano, Y. Abe, M. Hirabayashi, Acta Metall. 24 (1976) 95–96.